Design and analysis of 10MW 1+1/2 supercritical carbon dioxide counter-rotating turbine

Wu et al. Propulsion and Energy (2026) 2:7
https://doi.org/10.1007/s44270-026-00036-y

PROPULSION AND ENERGY

RESEARCH Open Access

Design and analysis of 10MW 1 + 1/2 supercritical carbon dioxide counter-rotating turbine

Longgang Wu[1], Chen Yang[1*], Xin Wei[1], Jinguang Yang[1], Dayong Wang[1] and Michele Ferlauto[2]

Abstract

In order to reduce the axial size of the supercritical carbon dioxide (SCO_2) Brayton cycle system and enhance its power-weight ratio, this paper proposes a counter-rotating design approach for SCO_2 turbines. The design process primarily involves 1D aerodynamic design based on theoretical analysis of velocity triangles and blade geometry modeling. A three-stage 10 MW SCO_2 axial turbine is selected as a test case and redesigned as a 1 + 1/2-stage counter-rotating turbine (CRT) configuration. Compared with the three-stage turbine, the axial length of the CRT is reduced by 63.5%. Subsequently, the performance of the designed counter-rotating SCO_2 turbine is validated through detailed numerical analysis utilizing the three-dimensional computational dynamics method, considering real gas effects of CO_2 by employing a physical property database for property calculations. The computational fluid dynamics results demonstrate that under design conditions, the isentropic efficiency is 92.4%, which represents a 12.4 percentage points improvement over the design target and satisfactorily meets the design objectives. Further analysis on the flow field was conducted, and it was found that the turbine streamlines are uniform, the entropy increase is concentrated at the trailing edge of the blades, and the average absolute outlet flow angle is 0° approaching the axial direction. The behavior of the CRT under off-design conditions is also discussed.

Keywords Counter-rotating turbine, SCO_2 turbine, Aerodynamic design, Numerical simulation

1 Introduction

The closed supercritical carbon dioxide (SCO_2) Brayton cycle system can provide higher efficiency and reduce carbon emissions for the power industry [1]. In addition, it has the outstanding merit of much higher power density, i.e., significantly smaller size compared to a traditional power plant. Among its components, the turbine plays an important role in the supercritical carbon dioxide Brayton cycle system, which directly affects the cycle efficiency and power generation efficiency. Therefore, the selection and design optimization of the turbine is very important [2].

Han et al. [3] proposed an improved coal-fired recompression SCO_2 Brayton cycle system, and provided a detailed introduction to the design and numerical simulation of a 5 MW SCO_2 turbine. Stepanek et al. [4] designed and optimized SCO_2 turbines for high-power cycles, achieving efficiencies comparable to steam turbines. The research also emphasized the significance of reducing the turbine size. Zhang et al. [5] designed a 1.5 MW radial turbine and a 15 MW axial turbine by combining the NIST physical program and the SCO_2 aerodynamic design program. Lv et al. [6] proposed an optimization design method that can predict various losses of the SCO_2 radial turbine, and the computational fluid dynamics (CFD) simulation results are in good agreement with the experimental results.

*Correspondence:
Chen Yang
yangchen@dlut.edu.cn
[1] School of Energy and Power, Dalian University of Technology, Dalian 116024, China
[2] Department of Mechanical and Aerospace Engineering, Politecnico di Torino, Turin 10129, Italy

Compared to a traditional axial turbine design, the counter-rotating turbine (CRT), benefitting from the counter-rotating concept, can fully take advantage of the pre-swirl generated by the upstream rotor, reducing the number of downstream turbine guide vanes, or even canceling the downstream guide vanes, which has the potential of further enhancing the power density and reducing the weight and cost of the SCO_2 plant.

As early as 1957, Wintucky et al. [7] analyzed the variation of 1 + 1/2 CRT efficiency with high and low-pressure turbine speed-to-power ratio, exit whirl, and other parameters. The research shows that the CRT is 2%–4% more efficient than the traditional turbine. Louis et al. [8] studied the design characteristics and off-design characteristics of 1 + 1/2 and 1/2 + 1/2 CRTs in 1985, and studied the variation of efficiency with load coefficient. Bellocq et al. [9] conducted zero-dimensional and one-dimensional design and performance analysis of the engine's multi-stage CRT, removing the guide vanes, greatly reducing the engine weight and improving efficiency. Rajeevalochanam et al. [10] designed a CRT to increase turbine power at the same mass flow rate, expansion ratio, inlet, and outlet conditions as a co-rotating turbine. The design results show that the performance of the CRT is improved by 2% at the design point.

A number of studies have also been carried out on the CRT in China. Cai et al. [11] and Ji et al. [12] carried out a detailed analysis of the elementary stage velocity triangle of the CRT and explored the preliminary design method of the CRT. Liu et al. [13] studied the influence of two-stage turbines' efficiency on the performance of the whole engine. They found that counter-rotating is able to change the flow field by changing positive swirl flow to negative swirl flow, which will help to increase turbine efficiency. Zhou et al. [14] analyzed the design parameters of the CRT, optimized the selection of the velocity triangle, and calculated the variation of the efficiency with the outlet flow angle. Fang et al. [15] completed the design of a high-load CRT with an expansion ratio of 5.69, and the efficiency of the CRT was 1.77% higher than that of the traditional turbine. Zhao et al. [16] carried out 1 + 1/2, 1 + 1, and 1 + 3/2 CRT elementary stage analysis, and discussed the through-flow design and three-dimensional aerodynamic design methods. An optimization scheme is also proposed for variable working conditions to make the turbine more stable under off-design conditions. Luo et al. [17] applied the CRT technology to the radial turbine and completed the aerodynamic design and numerical analysis of a 1 + 1/2 counter-rotating radial turbine. The results show that the maximum diameter of the 1 + 1/2 counter-rotating radial turbine is reduced by 12%. and the efficiency is increased by 1.57%.

Though great progress has been achieved in CRT design in the past decades, the studies mentioned above mainly focused on aero-engine applications. To the authors' best knowledge, research on the design of CRT for the SCO_2 Brayton cycle is still rare. Regarding the SCO_2 cycle, the turbomachinery components of the supercritical carbon dioxide cycle power plant are relatively small in size. However, the gas storage tanks, pipelines, and other devices are large in volume, which will largely offset the volume advantage brought by the turbomachinery components. Therefore, there is still a need to reduce the volume for SCO_2 cycle. Compared with a traditional axial turbine, the CRT studied in this paper can further reduce the volume while ensuring efficiency. While having the above advantages, ensuring high efficiency of the CRT remains a difficulty and challenge in its design.

This paper proposes a counter-rotating SCO_2 turbine design method. A 1D turbine design based on theoretical velocity triangle analysis was first carried out. Then, on the basis of the designed geometric parameters, the 3D blade geometry of the CRT was obtained. Taking the three-stage axial flow SCO_2 turbine designed by Kumaran et al. [18] as the prototype, a counter-rotating redesign was implemented to replace the prototype turbine with a 1 + 1/2 CRT. The numerical simulation results of the CRT design were analyzed. Finally, the main advantages of the SCO_2 CRT were summarized.

The differences in the research work of this paper are mainly reflected in: (1) the meanline design calculation process of the counter-rotating turbine under arbitrary working fluid conditions is re-sorted out and described; (2) compared with the traditional single-shaft configuration, the counter-rotating turbine features dual shaft speeds, resulting in more design variables and a larger design space. This fundamentally alters the velocity triangle matching law, particularly in multi-stage applications.

2 Turbine design

2.1 Turbine description

In the simple recuperative Brayton cycle system, the three-stage turbine serves as a core component, with the system integrating essential elements such as the compressor, recuperator, main heat exchanger, turbine, and gas cooler. Within this system, CO_2 operates under supercritical conditions. Based on the thermodynamic design points obtained from cycle calculations, we can conduct initial aerodynamic designs for both the prototype turbine and the CRT. This paper achieves the redesign of the three-stage turbine into a 1 + 1/2 CRT, and both designs strictly follow the same inlet and outlet conditions to ensure consistency and comparability. Subsequently, this paper will focus on elucidating the design process of the CRT, while providing only a concise description of the prototype turbine design to facilitate a comparative analysis with the design results of the CRT. The specific design parameters have been summarized as shown in Table 1.

2.2 Mean-line design

The physical properties of SCO_2 have a significant impact on the size and design specifications of the turbine, resulting in a turbine that is characterized by high power density and lower enthalpy. This is evidenced by the fact that the SCO_2 turbine has a smaller flow path and fewer stages. Despite the SCO_2 turbine's smaller dimensions compared to those of a typical aero-engine, its flow mechanism exhibits similarities to that of the aero-engine. Consequently, the design techniques originally employed for CRTs in aero-engines can be effectively applied to the SCO_2 turbine.

Table 1 Design parameters of the turbine [18]

Parameter	Value
Mass flow rate (kg/s)	104.8
Power (MW)	10
Isentropic efficiency (%)	80
Total-to-total pressure ratio	2.2
Inlet total pressure (kPa)	20350
Inlet total temperature (K)	818.5
Rotational speed (r/min)	12000

A 1 + 1/2 CRT typically consists of a row of 1st stage stators, 1st stage rotors, and 2nd stage rotors rotating in the opposite direction to the 1st stage rotors. Usually, the work distribution between the two stages of the CRT depends on the potential matching requirements of the counter-rotating compressor. Due to the lack of guide vanes in the 2nd stage turbine, under the target that the 2nd stage turbine outlet flow angle does not deviate from the axial direction, the power capacity of the 2nd stage turbine is limited by the fluid conditions at the outlet of the 1st stage turbine, so it is difficult for the 2nd stage turbine to achieve the design goal of the output power. Therefore, one of the design challenges is how to reduce the specific work ratio of 1st and 2nd stages [19]. Under axial exhaust conditions, to enhance the work capacity of the 2nd stage rotors, the 1st stage rotors must provide appropriate flow velocity and angle [20].

The typical flow path and station diagram of a 1 + 1/2 CRT is shown in Fig. 1. Stations 1, 2, 3, 4, and 5 are marked as stator inlet, rotor1 inlet, rotor1 exit, rotor2 inlet, and rotor2 exit, respectively.

Primarily, one-dimensional aerodynamic calculations are carried out for the 1st stage of the counter-rotating turbine. This design is a constant mean radius design, and the values of the stage enthalpy drop, flow coefficient, load coefficient, and axial velocity ratio need to be estimated at the beginning of the design. The initial stage inlet hub-tip ratio (r_{1t}/r_{1h}), the inlet Mach number (Ma_1), the first stage outlet hub-tip ratio (r_{3t}/r_{3h}), and the outlet total pressure (p_{03}) can be referred to the original turbine design results. The flow coefficient

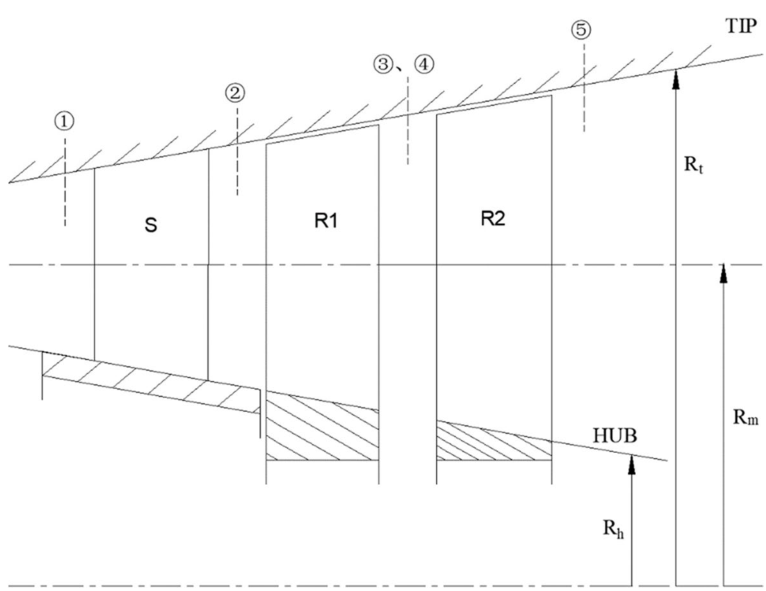

Fig. 1 Station diagram of 1+1/2 CRT

and load coefficient are expressed by Eqs. (1) and (2), respectively:

$$\phi = \frac{C_{2a}}{U_1} \tag{1}$$

$$\psi = \frac{\Delta h_{0\mathrm{stage1}}}{U_1^2} \tag{2}$$

According to the above equations, the axial velocity C_{2a} and inlet velocity U_1 of the rotor can be obtained:

$$U_1 = \sqrt{\frac{\Delta h_{0\mathrm{stage1}}}{\psi}} \tag{3}$$

$$C_{2a} = U_1 \times \phi \tag{4}$$

The blade inlet and outlet areas and blade height can be calculated according to the following equations:

$$A = \pi \times r_{\mathrm{t}}^2 \left[1 - \left(\frac{r_{\mathrm{h}}}{r_{\mathrm{t}}}\right)^2\right] \tag{5}$$

$$H_{\mathrm{blade}} = \frac{A}{2\pi \times r_{\mathrm{m}}} \tag{6}$$

The thermodynamic parameters of different stations of the turbine can be calculated from the REFPROP software. The state equations are:

$$[p, T] = f(h, s) \tag{7}$$

$$[\rho, c_p, k] = f(p, T) \tag{8}$$

The static enthalpy h_3 at the outlet of the rotor is calculated according to the state equations. The absolute velocity C_3 at the outlet of the rotor blade can be obtained from the relationship between the total enthalpy and the static enthalpy:

$$h_{03} = h_3 + \frac{1}{2}C_3^2 \tag{9}$$

With the absolute velocity C_3 of the rotor outlet defined, the tangential velocity component of the rotor blade outlet can be calculated by the following formula:

$$K_{23} = \frac{C_{3a}}{C_{2a}} \tag{10}$$

$$C_{3w} = \sqrt{C_3^2 - C_{3a}^2} \tag{11}$$

According to the trigonometric function relationship between the velocity and angle of the velocity triangle, the flow angle and relative velocity of the rotor outlet are obtained:

$$\alpha_3 = \arctan\left(\frac{C_{3w}}{C_{3a}}\right) \tag{12}$$

$$\beta_3 = \arctan\left(\tan\alpha_3 - \frac{U_1}{C_{3a}}\right) \tag{13}$$

$$W_3 = \frac{C_{3a}}{\cos\beta_3} \tag{14}$$

Assuming that the tangential velocity at the inlet and outlet of the rotor blade is constant, the tangential velocity at the inlet of the rotor blade can be obtained by Euler's work formula:

$$\Delta h_{0\mathrm{stage1}} = U_1(C_{2w} + C_{3w}) \tag{15}$$

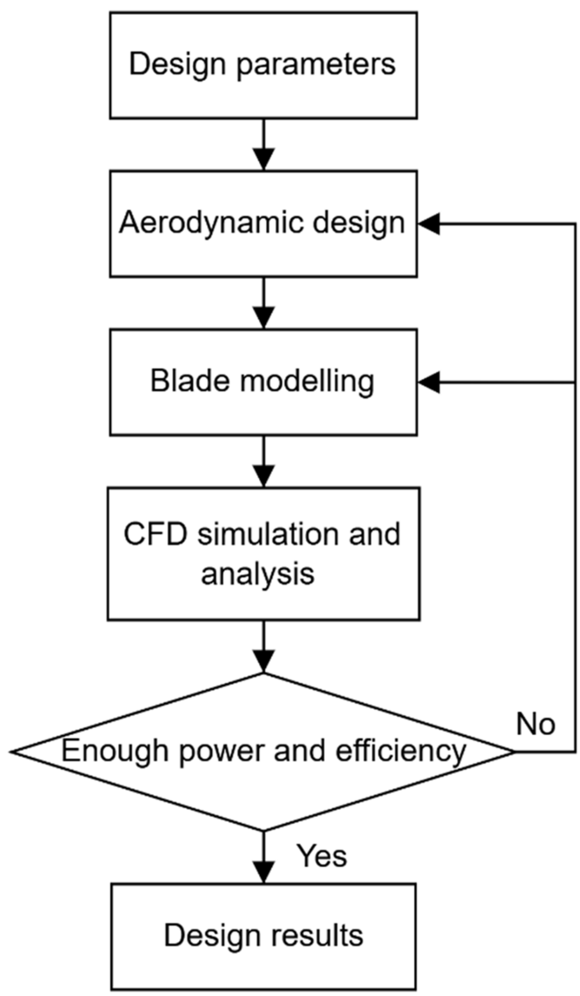

Fig. 2 Flow chart of the CRT design

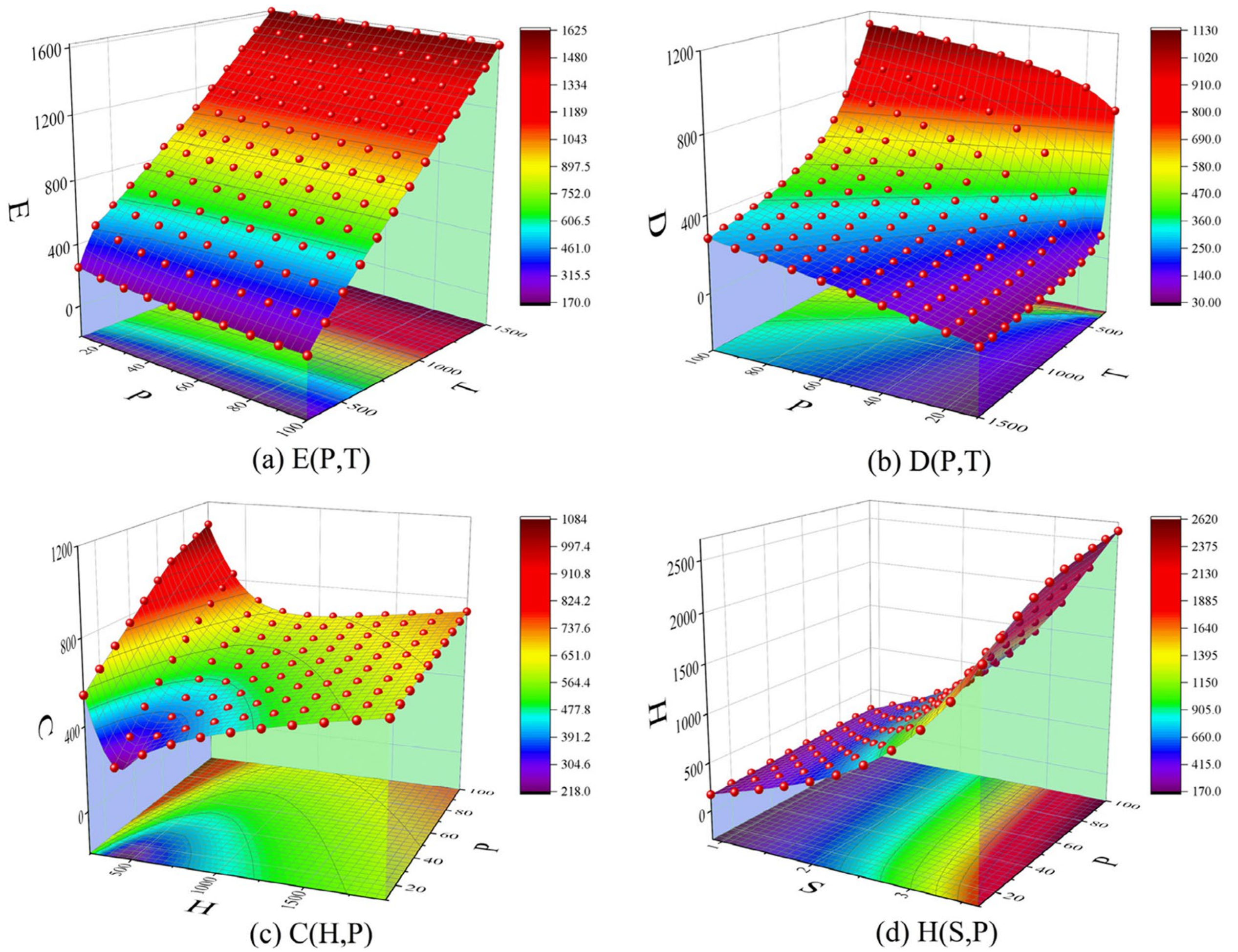

Fig. 3 The distribution of four physical properties data

Similarly, the inlet flow angle and flow velocity of the rotor can be obtained:

$$\alpha_2 = \arctan\left(\frac{C_{2w}}{C_{2a}}\right) \tag{16}$$

$$\beta_2 = \arctan\left(\tan\alpha_2 - \frac{U_1}{C_{2a}}\right) \tag{17}$$

$$C_2 = \frac{C_{2a}}{\cos\alpha_2} \tag{18}$$

$$W_2 = \frac{C_{2a}}{\cos\beta_2} \tag{19}$$

At this point, the velocity triangle of the 1st stage can be determined. By assuming that the axial velocity ratio of the 2nd stage $K_{45}=1$ and the outlet absolute flow angle $\alpha_5 \approx 1°$, the outlet angle and velocity of the rotor R2 can be obtained.

The total-to-total efficiency formula for evaluating the aerodynamic performance of a counter-rotating turbine is defined by Eq. (20):

$$\eta_{\rm tt} = \left[1 + \left(\frac{\zeta_{\rm S} C_2^2 \frac{T_3}{T_2} + \zeta_{\rm R1} W_3^2 + \zeta_{\rm R2} W_5^2}{2\Delta h_0}\right)\right]^{-1} \tag{20}$$

The loss model for the SCO_2 turbine is based on the AMDCKO loss model, which has gained widespread use in engineering. This model is based on the AMDC model. The AMDC loss model has good prediction accuracy under typical turbine operating conditions of aircraft engines, but it shows deviations in small turbines and non-typical turbine applications. To address this limitation, Kacker and Okapuu [21] improved the AMDC model [22].

Following the preliminary mean-line design of the 1st stage turbine, the inlet and outlet parameters of the 2nd stage rotor blade can be used to determine the 2nd stage turbine design. However, the axial speed ratio and rotational speed ratio between the 1st and 2nd stages must be estimated. In order to reduce losses, the absolute velocity of the outlet can be taken between the range of 0° and 5°. Figure 2 shows the design process of the counter-rotating turbine.

2.3 Physical properties of SCO_2 working fluid

Compared with other inert gases, CO_2 has relatively moderate critical parameters, with a critical pressure of 7.38 MPa and a critical temperature of 31.1 °C (304.25 K), which is close to room temperature, stable, and abundant. When the temperature and pressure values of CO_2 are higher than the critical values, CO_2 enters the supercritical state.

In order to accurately calculate the physical properties of the real CO_2 gas, the NIST-REFPROP physical property database was consulted to obtain a detailed physical property file for CO_2 gas. The file is employed in the mean-line design and numerical calculations of the SCO_2 CRT. Before the numerical calculations, the TabGen module of NUMECA is employed to generate a folder of physical property data sheets that can be identified and utilized by the FINE/Turbo solver for simulating the actual SCO_2 flow model.

Figure 3 shows the distribution of four physical properties data generated by TabGen, which are internal energy (E) data $E(p, T)$ with pressure (p) and temperature (T) as variables, density (D) data $D(p, T)$ with p and T as variables, thermal conductivity (K) data $K(H, p)$ with enthalpy (H) and p as variables, $H(S, p)$ with entropy (S) and p as variables.

Table 2 Aerodynamic design results of CRT

Parameter	First stage	Second stage
Rotational speed (r/min)	12000	10000
Flow coefficient	0.33	0.7
Loading coefficient	2.74	1.25
Reaction	0.55	1
Number of blades	23/24	24
Solidity	1.24/1.28	1.28
Specific work (MW)	7.62	2.42
Axial length (mm)	109.4	
Specific work ratio	3.15	
Isentropic efficiency (%)	87.6	
Power (MW)	10.04	

Table 3 Results of flow angle and tip clearance

Parameter	S1	R1	R2
Absolute flow angle at the outlet (°)	77.38	62.34	1.1
Relative flow angle at the outlet (°)	77.38	75.12	56.42
Tip clearance (mm)	-	0.098	0.138

2.4 Aerodynamic design results

This paper explores in depth the mean-line design methodology for CRTs by parametrically adjusting key parameters such as axial velocity ratio, load coefficient, and rotational speed ratio. Based on the design parameters listed in Table 1, the aerodynamic design was carried out for the 1 + 1/2 CRT and the three-stage turbine with CO_2 real gas as the working fluid. Given that the thermodynamic properties of SCO_2 are more complex compared to ideal gases, the NIST-REFPROP physical property database was utilized to calculate the thermodynamic properties of CO_2 under different conditions.

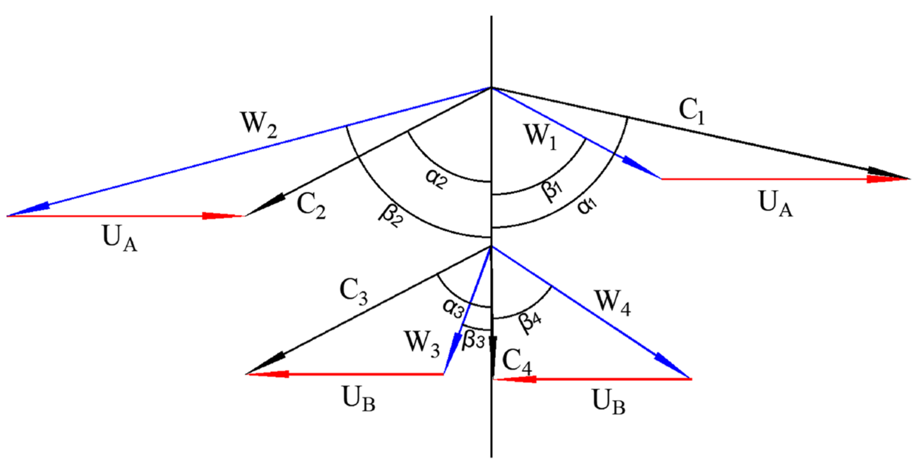

Fig. 4 Velocity triangle

It is required that the blade size and number of the CRT match those of the three-stage turbine, and both adopt a constant mean diameter design. This design strategy helps to highlight the significant advantages of CRTs in reducing axial length and weight. The results of the one-dimensional aerodynamic design of the CRT are shown in Tables 2 and 3, in which the rotational speed ratio of the CRT is 1.2, the specific work ratio is 3.15, and the isentropic efficiency is 87.6%, which is 7.6 percentage points higher than the design target. Furthermore, the output power reaches the target. To visually represent the aerodynamic parameters, the velocity triangle of the CRT

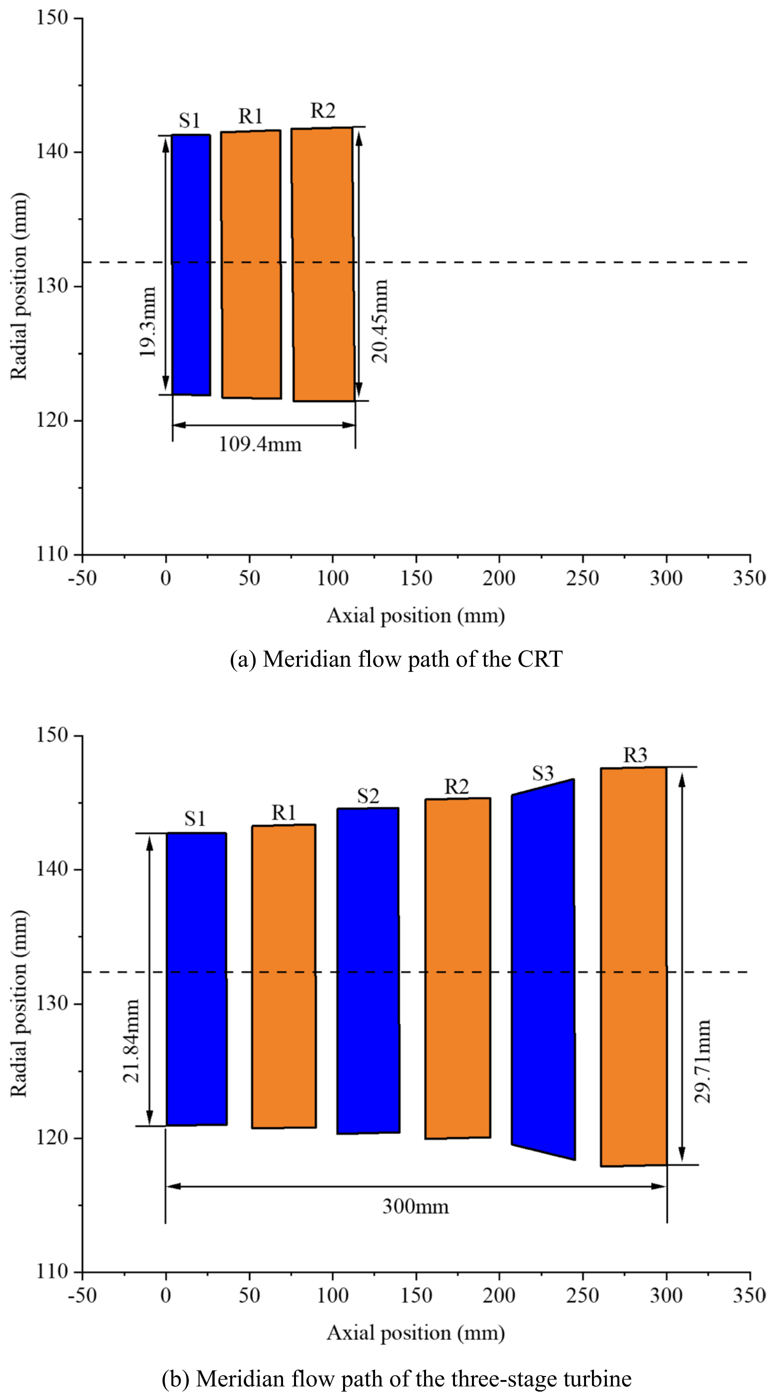

(a) Meridian flow path of the CRT

(b) Meridian flow path of the three-stage turbine

Fig. 5 Meridian flow path

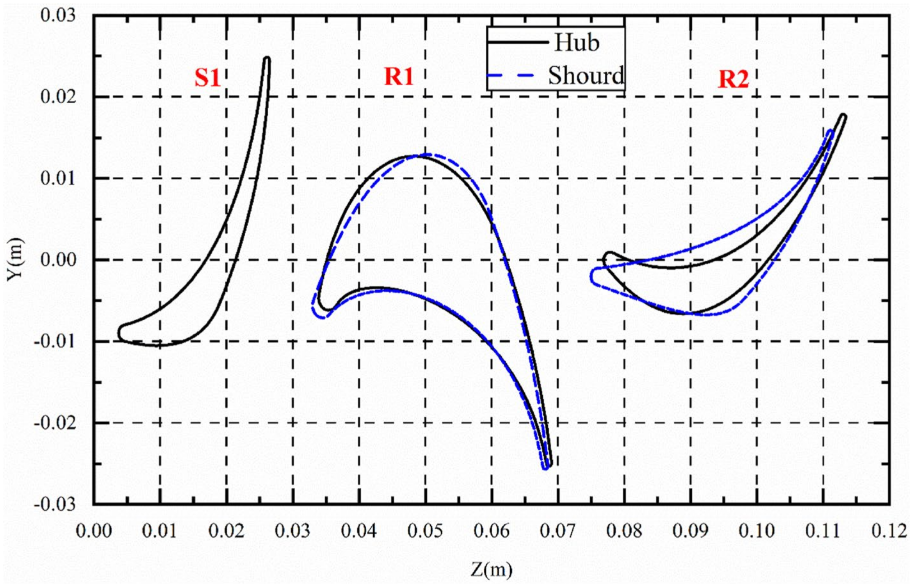

Fig. 6 Blade profiles at hub and tip

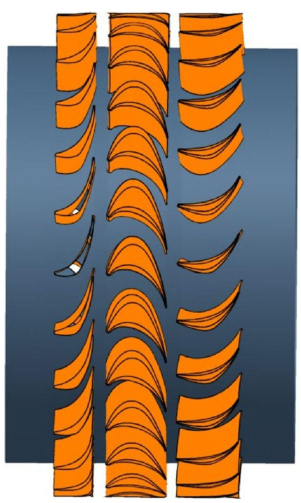

Fig. 7 Three-dimensional geometry of CRT

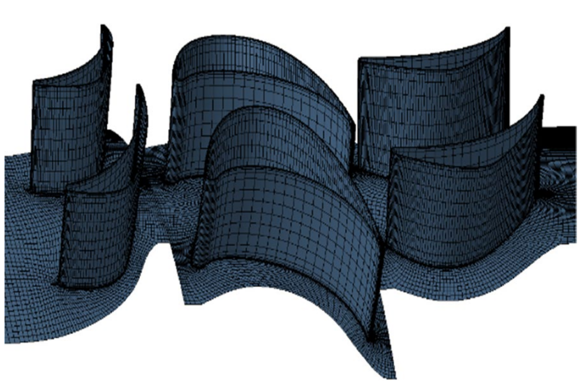

Fig. 8 Mesh division

is illustrated in Fig. 4, with an axial velocity ratio of 1.4 for the 1st stage and approximately 1 for the 2nd stage.

In Fig. 5(a), the meridional flow path height of the CRT remains constant. This design allows for an increase in the axial velocity ratio, effectively reducing the specific work ratio. In Fig. 5(b), the hub radius of the three-stage turbine is approximately 121 mm, and the inlet height of the blades is 21.84 mm. Through comparison, it is evident that the CRT has only half as many rows of blades. The 1 + 1/2 CRT has three fewer rows of blades than the three-stage turbine, and its axial length has been significantly shortened from the original 300 to 109.4 mm,

Table 4 Mesh independence verification

Mesh number (million)	1.87	2.05	2.30	2.66	3.00
Total-to-total pressure ratio	2.187	2.187	2.188	2.19	2.19
Mass flow rate (kg/s)	104.55	104.57	104.59	104.6	104.6
Isentropic efficiency (%)	90.6	91.9	92.3	92.4	92.43

Table 5 Comparison of CFD and mean-line design results

	Design target	Mean-line design	CFD	Difference (%)
Total-to-total pressure ratio	2.2	2.2	2.2	-
Mass flow rate (kg/s)	104.8	104.8	104.6	−0.19
Isentropic efficiency (%)	80	87.6	92.4	5.48

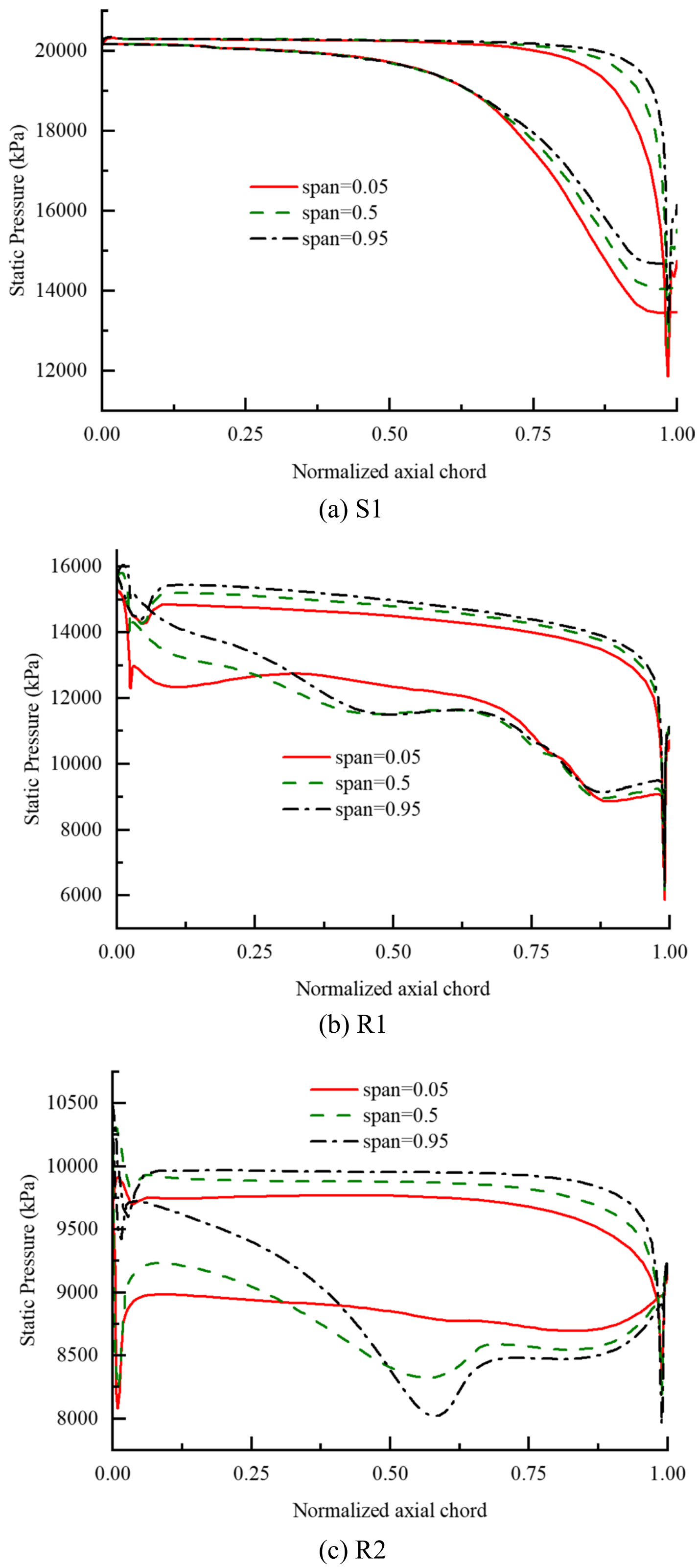

Fig. 9 Static pressure distributions at different spanwise sections

a reduction of 63.5%. This design not only significantly reduces the axial size and weight of the turbine but also achieves cost savings.

2.5 Blade modelling

To reduce the size deviation between the CRT and the three-stage turbine, the blade height and hub height of the CRT were controlled within an appropriate range.

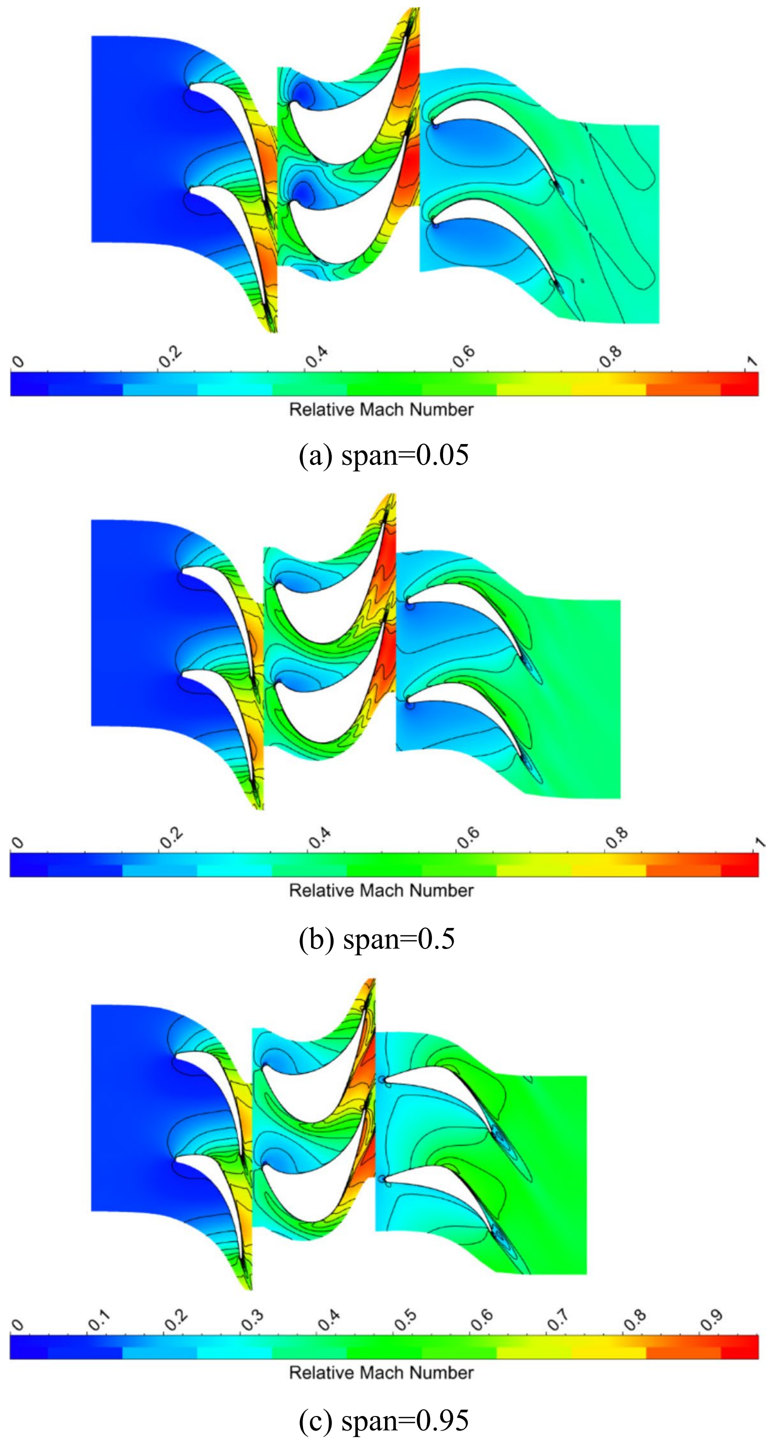

Fig. 10 The relative Mach number at different spanwise sections

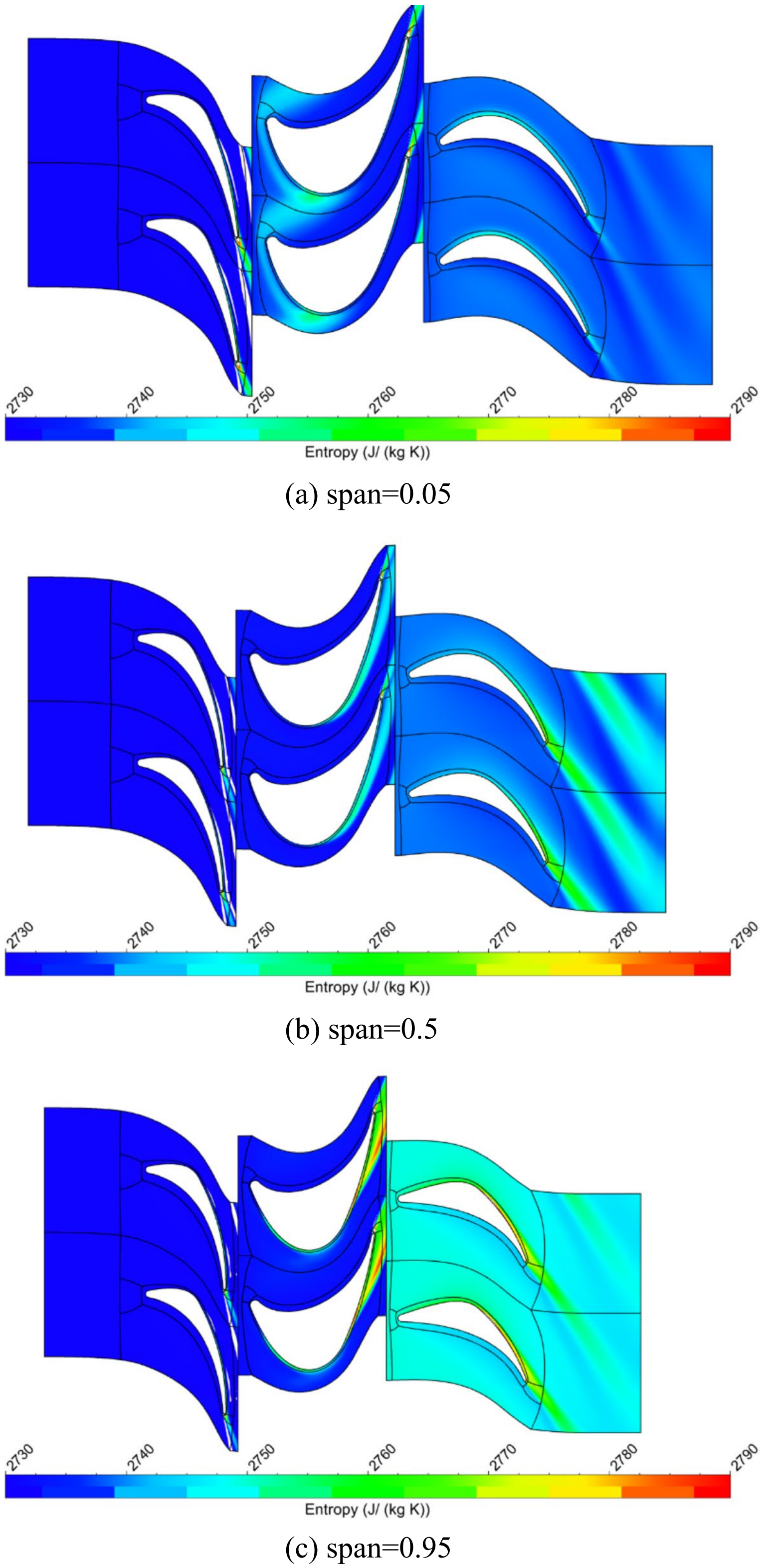

Fig. 11 The entropy at different spanwise sections

In the design of the flow path, a constant mean diameter design method was adopted. This strategy effectively decreased the expansion angle of the flow path of the turbine, thereby increasing the axial velocity ratio. Meanwhile, a rear-loaded blade profile was chosen in the blade design to minimize aerodynamic losses.

At the tip of the blade, the rotor is equipped with a shroud to reduce the leakage loss at the blade tip. Although the blade was relatively small and belonged to the category of traditionally defined short blades, due to the significant variation of the rotor reaction along the radial direction, we employed curved and twisted blades to reduce the leading-edge incidence angle and thus improve flow characteristics. However, this design also correspondingly increased the difficulty and cost of industrial processing. Taking into account the factory's processing capabilities, the trailing edge thickness of the blade was set to 0.8 mm, and the blade was generated using a stacking method based on the center of gravity.

The final blade profiles at the hub and tip of the CRT are shown in Fig. 6. In Fig. 6, S1, R1, and S2 represent the first-stage stator, the first-stage rotor, and the second-stage counter-rotating rotor, respectively. In Fig. 6, S1 adopts a straight blade design with a consistent blade profile from hub to tip, while two rows of counter-rotating rotors, both utilizing curved and twisted blade designs. Finally, the three-dimensional geometry of the blades stacked by different spanwise section blade profiles is shown in Fig. 7.

3 Numerical simulation

3.1 Mesh generation

Numerical calculations were conducted in NUMECA software, using the AutoGrid module for meshing. The mesh division is shown in Fig. 8. The H-O-H multi-block structured grid was selected for the computational mesh. To ensure the accuracy of numerical calculations, the mesh at the wall intersections was refined. Additionally, a triple-grid partitioning technique was employed to accelerate convergence. To ensure that the calculation results are independent of the number of meshes, the independence of the mesh was verified. The mesh independence verification is shown in Table 4. The results indicated that when the total number of meshes is greater than 2.66 million, the results are stable and unchanged at the design point, and it can be assumed that the calculation results are independent of the number of meshes. In order to speed up the calculation, a mesh of 2.66 million was selected for CFD numerical calculation in this paper, and the meshes of each row of blades are about 0.7 million, 0.96 million, and 1 million, respectively, and the y^+ value of the mesh in the calculation process is less than 15.

3.2 Numerical calculation setting

The turbine blade and solid wall boundary conditions are selected as non-slip and adiabatic. The computations are performed using the FINE/Turbo solver to solve the steady Navier–Stokes (N–S) equations. The spatial discretization is carried out using a central difference scheme, while the time discretization employs a fourth-order Runge–Kutta method for iterative solutions. The turbulence model adopted is the Spalart–Allmaras model. During the computation process, an implicit residual smoothing method and multi-grid technology are utilized to accelerate convergence. The boundary conditions are set with a total inlet temperature of 818.5

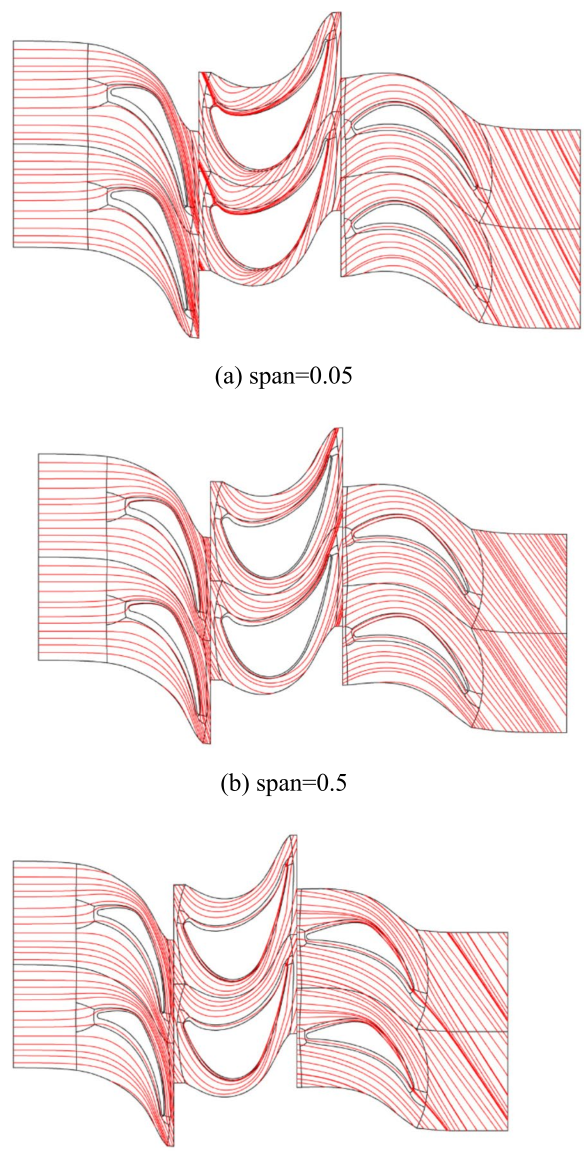

(a) span=0.05

(b) span=0.5

(c) span=0.95

Fig. 12 The streamlines at different spanwise sections

K, a total inlet pressure of 20350 kPa, and a static outlet pressure of 8925.44 kPa.

4 Result analysis

4.1 Calculation results

The results of the three-dimensional calculations are listed in Table 5 for comparison with the one-dimensional calculations. The CFD results show that at the same total-to-total pressure ratio, the mass flow rate is 0.19% smaller and the efficiency is 4.8 percentage points higher than those predicted by mean-line design, which satisfies the preliminary design requirements. This difference in efficiency mainly results from two aspects: the geometry deviations introduced during the subsequent

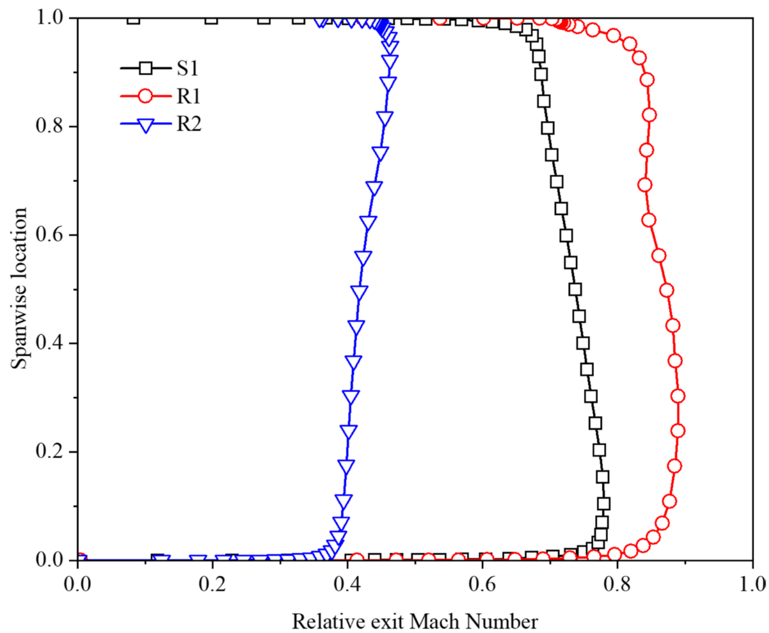

(a) Relative exit Mach number

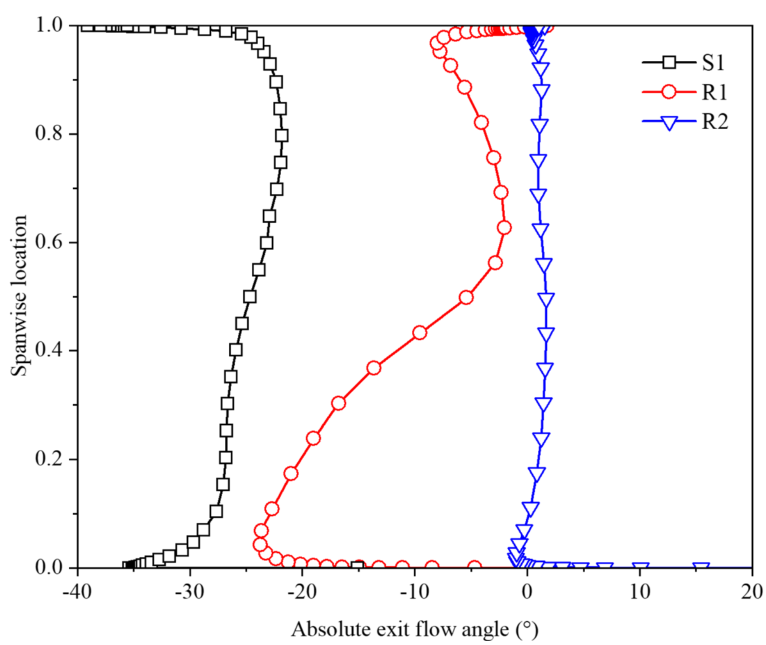

(b) Absolute exit flow angle

Fig. 13 Relative Mach number and absolute flow angle distribution along the span

3D blade modeling, and the prediction error of the current empirical model. Overall, the mass flow rate difference is negligible, while the efficiency validated by CFD is 12.4 percentage points higher than the design target, which is a very significant increase. Consequently, the primary parameters of the CRT satisfy the design target.

4.2 Flow field analysis of counter-rotating turbine

Figure 9 shows the static pressure distributions at different spanwise sections. A significant over-expansion region is observed at the trailing edge of the three rows of blades, which can be attributed to the considerable thickness of the trailing edge and the rapid expansion of boundary layer flow on the pressure surface. Along the axial chord length, the static pressure on the stator blade surface is observed to decrease gradually. Over-expansion occurs on both sides of the leading edges of the 1st and 2nd stage rotors because the curvature of the leading edges of the blades is too large, the area of the flow path is reduced, and the CO_2 enters the flow path and accelerates through it. Although there is a slight adverse pressure gradient on the rotor suction surface, it does not significantly affect the flow process.

From the relative Mach number cloud diagram in Fig. 10, it can be observed that the maximum Mach number occurs in the throat of the 1st stage rotors, and there exists a localized supersonic region with a maximum Mach number of 1.2. CO_2 flows fully within the stator blades, with the Mach number gradually decreasing from the blade hub to the tip. At the 75% chord length position on the suction surface of the 1st stage rotor blades, the CO_2 reaches supersonic speed, and local supersonic regions exist from the blade hub to the tip. For the 2nd stage rotors, there is almost no change in the Mach number of the suction and pressure surfaces at the hub, which is consistent with their static pressure distribution at the hub. From the hub to the tip of the blade, the wake of the 2nd stage rotors gradually becomes larger, and the loss in this area also increases.

Figure 11 shows the entropy distribution at different spanwise sections of the CRT. The increase in entropy represents the increase in loss. From Fig. 11, it can be seen that the losses are increasing from the hub to the tip of the blade and are mainly concentrated at the trailing edge of the rotors. This is due to the thicker trailing edge, forming a larger boundary layer, resulting in increased losses.

The streamlines at different spanwise sections in Fig. 12 are smooth, indicating that the flow condition in the turbine passage is satisfactory and there is no large-scale separation. Only in the span = 0.05 section do the streamlines in the 1st stage rotor converge to the suction surface and flow out along the trailing edge of the suction surface.

Figure 13 shows the distribution of the relative Mach number and absolute flow angle at the outlet of each row of blades along the spanwise direction. The distribution of the Mach number at the outlet of each row of blades is uniform along the spanwise direction, with average values of 0.73, 0.86, and 0.43 for S1, R1, and R2, respectively. The relative Mach number at the outlet of the R1 is maximum, and all the Mach numbers are less than 0.9 along the spanwise distribution.

In the spanwise direction, the absolute outlet flow angle distribution of R1 is relatively uniform from the 60% spanwise position to the blade tip. However, a notable change in the flow angle is observed below the 60% spanwise position, with a shift from approximately −2° to approximately −23°. This discrepancy in the distribution of the flow angle along the spanwise direction is

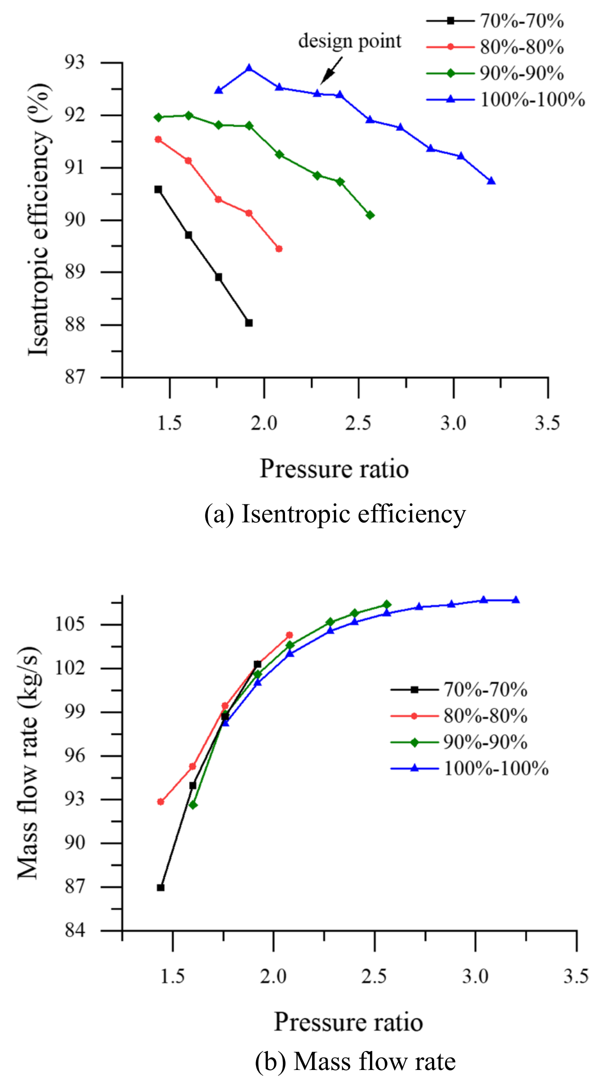

Fig. 14 Off-design characteristics of CRT

considerable, which results in a notable alteration in the inlet angle of the R2 along the spanwise direction and ensures that the absolute outlet flow angle of R2 exhibits a near-zero value and a highly uniform distribution fulfilling the design work output.

5 Off-design point operating characteristics

The isentropic efficiency and mass flow rate have been analyzed by numerical calculations at five sets of speeds from 70% to 100% and at different pressure ratios of operating conditions. As shown in Fig. 14, the horizontal coordinates of the graph are the total-to-total pressure ratios, and the location of the design point is indicated. In Fig. 14(a), the 1st and 2nd stage turbines' rotors maintain high efficiencies above 90% at both 90% and 100% speed. The turbine efficiency decreases with increasing pressure ratio at different speeds, and the decreasing trend in efficiency increases with decreasing speed. The turbine efficiency is highest at 100% design speed, and the highest point of efficiency is at a pressure ratio of 1.92. The lowest efficiency is achieved at 70% design speed with a pressure ratio of 1.92. Figure 14(b) shows the flow characteristics of the CRT. The mass flow rate at different speeds follows the same trend; when the pressure ratio is greater than 2.88, the mass flow rate is almost unchanged as the turbine approaches choke condition. Overall, the CRT maintains high efficiency at different pressure ratios and therefore has excellent operating characteristics at the off-design point.

The decrease in efficiency at low speed is due to the change in incidence angle and relative inlet Mach number, which affects the accelerated flow in the blade passages. Figure 15 shows the streamlines and relative Mach number of the rotor at 70% design speed and a pressure ratio of 1.92. The incidence angle of R2 and R3 did not approach their design angles. The flow hit the pressure surface, and the inlet flow angle was a larger positive incidence angle. Therefore, flow separation occurs near the suction leading edge. However, as the incidence angle is almost 0 at design speed, there is no such phenomenon in the rotor passages.

6 Conclusion

In this paper, the CRT technology was applied to the SCO_2 turbine design. A 1 + 1/2 CRT was designed based on the rigorous analysis and elaborate selection of velocity triangles, aiming to replace a three-stage SCO_2 turbine. Specific blade design and numerical simulation were conducted for the designed CRT. The turbine flow field was analyzed in detail. The simulated off-design performance was also presented. The conclusions are as follows:

(1) When designing a CRT, it is necessary to comprehensively consider not only the specific work ratio

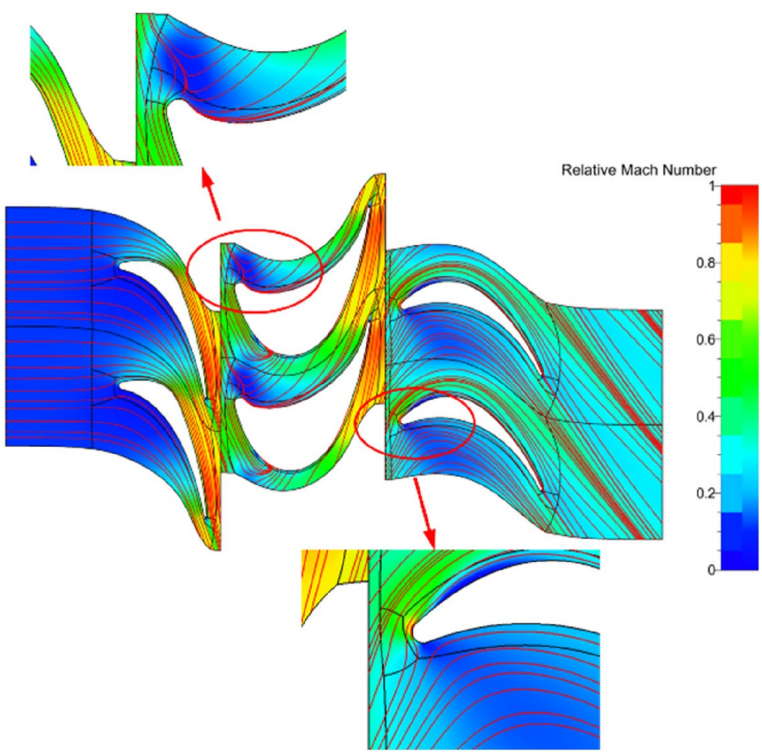

Fig. 15 Streamlines and relative Mach number at 70% speed with a pressure ratio of 1.92

between the 1st and 2nd stage turbines and the axial velocity ratio, but also the gas properties of SCO_2.

(2) In the design results, both the pressure ratio and the mass flow rate of the CRT achieved the design target satisfactorily, with 12.4 percentage points more efficiency than the design target. Under off-design point conditions, the efficiency of the CRT can still remain higher than 90% at 90% and 100% design speed, showing it can maintain excellent performance in the wide operating range.

(3) Under the premise of meeting the design targets, the $1+1/2$ CRT has three fewer blade rows than the prototype three-stage turbine, and at the same time, its axial length has been significantly shortened by 63.5%. This counter-rotating design is supposed to not only significantly reduce the weight of the turbine, but also effectively reduce material costs.

It should also be noted that the loss of CRT mainly results from the 1st stage turbine. Therefore, further improvement in the efficiency of the CRT is possible through an optimization design for the 1st stage turbine in future work.

Abbreviations

C	Sound speed, m/s
CFD	Computational fluid dynamics
CRT	Counter-rotating turbine
D	Density, kg/m^3
E	Internal energy, J/kg
h	Enthalpy, J/kg
K	Thermal conductivity, W/(m·K)
p	Pressure, Pa
SCO_2	Supercritical carbon dioxide
T	Temperature, K

Authors' contributions

Longgang Wu: Conceptualization, Software, Formal analysis, Writing original draft. Chen Yang: Methodology, Validation, Formal analysis. Xin Wei: Investigation, Data curation. Jinguang Yang: Resources, Supervision, Project administration. Dayong Wang: Supervision, Writing review. Michele Ferlauto: Supervision, Methodology, Writing editing. All authors read and approved the final manuscript.

Data availability

Data will be made available on reasonable request.

Declarations

Competing interests

Prof. Jinguang Yang is one of the editorial board members. The authors have no other competing interests to declare that are relevant to the content of this article.

Received: 24 October 2024 Revised: 24 December 2025 Accepted: 14 February 2026
Published online: 01 July 2026

References

1. Crespi F, Gavagnin G, Sánchez D et al (2017) Supercritical carbon dioxide cycles for power generation: a review. Appl Energy 195:152–183. https://doi.org/10.1016/j.apenergy.2017.02.048
2. Ye X, Pan W, You Y (2017) Application of supercritical carbon dioxide Brayton cycle in power generation fields. Power Energy 38(3):343–347
3. Han W, Zhang Y, Li H et al (2019) Aerodynamic design of the high pressure and low pressure axial turbines for the improved coal-fired recompression SCO_2 reheated Brayton cycle. Energy 179:442–453. https://doi.org/10.1016/j.energy.2019.05.016
4. Stepanek J, Syblik J, Entler S (2022) Axial sCO_2 high-performance turbines parametric design. Energy Convers Manag 274:116418. https://doi.org/10.1016/j.enconman.2022.116418
5. Zhang H, Zhao H, Deng Q et al (2015) Aerothermodynamic design and numerical investigation of supercritical carbon dioxide turbine. No. ASME GT2015-42619
6. Lv G, Yang J, Shao W et al (2018) Aerodynamic design optimization of radial-inflow turbine in supercritical CO_2 cycles using a one-dimensional model. Energy Convers Manag 165:827–839. https://doi.org/10.1016/j.enconman.2018.03.005
7. Wintucky WT, Stewart WL (1958) Analysis of two-stage counterrotating turbine efficiencies in terms of work and speed requirements. No. NACA-RM-E57L05
8. Louis JF (1985) Axial flow contra-rotating turbines. No. ASME 85-GT-218. https://doi.org/10.1115/85-GT-218
9. Bellocq P, Garmendia I, Legrand J et al (2016) Preliminary design and performance of counter rotating turbines for open rotors: Part II—0-D methodology and case study for a 160 PAX aircraft. No. ASME GT2016-57921
10. Rajeevalochanam P, Sunkara SNA, Murthy SVR et al (2020) Design of a two spool contra-rotating turbine for a turbo-fan engine. Propuls Power Res 9(3):225–239. https://doi.org/10.1016/j.jppr.2020.08.001
11. Cai R, Wu W, Fang G (1992) Basic analysis of counter-rotating turbines. Int J Turbo Jet Eng 9(1):1–10. https://doi.org/10.1515/TJJ.1992.9.1.1
12. Ji L, Zhong WT, Xu JZ (2001) Primary analysis and design of a vaneless counter-rotating turbine. J Eng Thermophys 22(2):167–170
13. Liu Y, Zhuge W, Zheng X et al (2013) Study of mechanism of counter-rotating turbine increasing two-stage turbine system efficiency. Int J Fluid Mach Syst 6(3):160–169. https://doi.org/10.5293/IJFMS.2013.6.3.160
14. Zhou Y, Liu H, Li W et al (2011) Aerodynamics design of two-stage vaneless counter-rotating turbinec. J Therm Sci 20:406–412. https://doi.org/10.1007/s11630-011-0488-z
15. Fang X, Liu S, Wang P (2005) Design and analysis of LP-vaneless contra-rotating turbine. J Propuls Technol 26(141):234–238. https://doi.org/10.3321/j.issn:1001-4055.2005.03.010
16. Zhao W, Sui XM, Zhao QJ (2020) Counter-rotating turbine flow mechanism and aerodynamic design. Sci Sin Technol 50:1376–1390
17. Luo D, Sun X, Huang D (2020) Design of 1 + 1/2 counter rotating centrifugal turbine and performance comparison with two-stage centrifugal turbine. Energy 211:118628. https://doi.org/10.1016/j.energy.2020.118628
18. Kumaran R S, Alone D B, Nassar A et al (2021) Preliminary aerodynamic design of a S-CO_2 axial turbine. No. ASME GTINDIA2021-76454
19. Yang Z, Huoxing L, Wei L et al (2011) Aerodynamics design of two-stage vane-less counter-rotating turbinec. J Therm Sci 20(5):406−412. https://doi.org/10.1007/s11630-011-0488-z
20. Zhao W, Wu B, Xu J (2015) Aerodynamic design and analysis of a multistage vaneless counter-rotating turbine. J Turbomach 137(6):061008. https://doi.org/10.1115/1.4028871
21. Kacker SC, Okapuu U (1982) A mean line prediction method for axial flow turbine efficiency. J Eng Power 104(1):111–119
22. Dunham J, Came PM (1970) Improvements to the Ainley−Mathieson method of turbine performance prediction. J Eng Power 92(3):252–256. https://doi.org/10.1115/1.3445349

Publisher's Note